Title
Development of PSMA Targeted Polymer Nanoparticles to Treat Prostate Cancer By Boron Neutron Capture Therapy Directed Against PSMA

Author
Dhrona, Suchi

Publication Date
2021

Peer reviewed|Thesis/dissertation

Development of PSMA Targeted Polymer Nanoparticles to Treat Prostate Cancer by Boron Neutron Capture Therapy Directed against PSMA

by
Suchi Dhrona

THESIS
Submitted in partial satisfaction of the requirements for degree of
MASTER OF SCIENCE

in

Biomedical Imaging

in the

GRADUATE DIVISION
of the
UNIVERSITY OF CALIFORNIA, SAN FRANCISCO

Approved:

DocuSigned by:
Flavell, Robert
DE54D221721B45E...
Flavell, Robert
Chair

DocuSigned by:
Henry F. VAnBrocklin
Henry F. VAnBrocklin

DocuSigned by:
Michael Evans
Michael Evans

DocuSigned by:
Youngho Seo
C525AA918D85484...
Youngho Seo

Committee Members

DEDICATIONS AND ACKNOWLEDGEMENTS

The completion of this study could not have been possible without the expertise of Dr. Robert Flavell, my thesis adviser, and my co-mentor, Niranjan Meher of Department of Radiology & Biomedical Imaging, University of California San Francisco. Their continuous support, guidance and overall insights in this field have made this an inspiring experience for me. Thank you to my committee members, Dr. Youngho Seo, Dr. Henry VanBrocklin and Dr. Micheal Evans. Your encouraging words and thoughtful, detailed feedback have been very important to me. I would also like to thank an American Cancer Society Individual Research Grant (IRG-97-150-13) and the New Directions in Prostate Cancer Research Award of the University of California, San Francisco Prostate Cancer Research Program for their support. The publication was supported by the Hellen Diller Family Comprehensive Cancer Centre Support Grant of the National Institutes of Health under P30 CA 82103. R.R.F was supported by the David Blitzer Young Investigator Award of the Prostate Cancer Foundation and a Physician Research Training Grant from the Department of Defense (PC 150932). A Pilot Grant by the Department of Radiology & Biomedical Imaging, University of California San Francisco also supported the research. A special thanks to Dr. Rob Franks and Dr. Brian Dreyer of the Marine Analytical Laboratory at the University of California, Santa Cruz, for their assistance with ICP-OES measurements. Finally, my deep and sincere gratitude to my family for their continuous and unparalleled love, help and support.

Development of PSMA Targeted Polymer Nanoparticles to Treat Prostate Cancer by Boron Neutron Capture Therapy Directed against PSMA

Suchi Dhrona

ABSTRACT

Prostate-specific membrane antigen (PSMA) is a cell surface enzyme highly over expressed in prostate cancer cells that can be employed as a target for prostate cancer imaging and drug delivery. Boron Neutron Capture Therapy (BNCT) is an emerging noninvasive therapeutic modality for treating locally invasive malignant tumors by selective delivery of high boron content to the tumor and then subjecting the tumor to epithermal neutron beam radiation. In this study, we develop carborane encapsulated amphiphilic polymer nanoparticles by conjugating urea based PSMA inhibitors (ACUPA) and ^{89}Zr chelating deferoxamine B (DFB) ligand and have investigated their efficacy to deliver enhanced boron payload to PSMA positive prostate cancer cells with simultaneous positron emission tomography (PET) imaging. Three different carborane encapsulated PLGA-b-PEG nanoparticles (NPs) were formulated with and without the PSMA targeting ligand, out of which two selected formulations; DFB(25)ACUPA(75) NPs and DFB(25) NPs radiolabelled with 89Zr were administered to mice bearing dual PSMA(+) PC3-Pip and PSMA(-) PC3-Flu xenografts. PET imaging and biodistribution studies were performed to demonstrate the in vivo uptake in mice. The NPs showed 2-fold higher uptake in PSMA(+) PC3-Pip tumors to that of PSMA(-) PC3-Flu tumors with a very high tumor/blood ratio of 20. However, no significant influence of the ACUPA ligands were observed. Additionally, the NPs demonstrated fast release of carborane with low delivery of boron to tumors in vivo. Although the in vivo efficacy of those NPs remain limited, a significant progress towards the synthesis, characterization and initial biological evaluation of the polymer nanoparticles is proposed in this report and the

results presented could guide the future design of amphiphilic polymer NPs for theranostic applications.

Keywords: boron neutron capture therapy (BNCT), prostate-specific membrane antigen (PSMA) inhibitor, ^{89}Zr, nanoparticles, amphiphilic block copolymer, positron emission tomography (PET) imaging

Table of Contents

List of Figures

List of Tables

List of Abbreviations

ACUPA: ((S)-2-(3-((S)-5-amino-1-carboxypentyl) ureido) pentanedioic acid

BNCT: boron neutron capture therapy

DCM: dichloromethane

DFB: deferoxamine B

EPR: Enhanced permeability and retention

FBS: fetal bovine serum

FDA: Food and Drug Administration

IACUC: Institutional Animal Care & Use Program

ICP-OES: inductively coupled plasma optical-emission spectrometry

iTLC: instant thinlayer chromatography

NPs: nanoparticles

PBS: phosphate-buffered saline

PCa: prostate cancer

PET: positron emission tomography

PSMA: prostatespecific membrane antigen

PVA: polyvinyl alcohol

ROI: region of interest

1. Introduction:

BNCT is a type of radiotherapy, which holds the potential to become a significant treatment for numerous types of tumors. BNCT is characterized by the neutron capture-fission response that happens when the stable isotope boron-10 (^{10}B) is radiated by low-energy (0.025 eV) thermal neutrons or epithermal neutrons (10,000 eV), which become thermalized as they pierce tissues. The higher energy neutron beam allows for the penetration of thick tissues and the skull, which is critical for BNCT success. In response to ^{10}B neutron capture, the consequent unstable ^{11}B isotope undergoes a nuclear fission response (^{10}B(n,a)^{7}Li) to produce an alpha particle (^{4}He), lithium-7 (^{7}Li) ion and gamma radiation equal to 2.31 MeV (94% of time) or 2.79 MeV (6% of time). The extent of cell disruption is restricted by the path lengths of the above-mentioned longitudinal energy transfer molecules, characteristically 4–10 mm, meaning their energy deposition is confined to an individual cell. ***(Fig.1.1)*** [1,2] Thus, this binary cancer treatment uses selective and optimum uptake of boron-containing drugs into cancer cells over normal cells, followed by selective neutron beam exposure to destroy the cancer cells.[3] As a result, BNCT has gained popularity for treating diseases like glioblastoma, melanoma, and head and neck cancers.[4,5] In contrast to head and neck cancers and glioma, BNCT has not been successfully applied in prostate cancer due to lack of suitable targeting probes despite some prior preliminary efforts.[6-8] However, the field currently suffers from a lack of boron delivery agents with high target to background ratio.[1,2,9] To achieve a successful BNCT therapy, it is necessary to deliver approximately ~20–50 μg of ^{10}B per gram of tumor (~10^{9} atoms/cell) and a sufficient

Figure 1.1. Schematic presentation of BNCT

amount of neutrons must penetrate and be absorbed by the cells to initiate a fatal ^{10}B (n, a)^{7}Li fission reaction.[10]

Prostate cancer is one of the most prevalent noncutaneous cancer in men. PSMA is a cell surface enzyme which is highly expressed on the prostate cancer cells, low in normal prostate, and expressed to varying extents in other normal tissues.[11,12] Recently, urea-based inhibitor agents targeting the enzymatic domain of PSMA have been developed for both imaging and therapy of prostate cancer.[13,14] Theranostic agents that can target PSMA with radionuclides, including ^{177}Lu and ^{225}Ac, are currently under investigation for treatment of metastatic prostate cancer. Indeed, the recently published VISION and TheraP trial results demonstrate a clear benefit of 177Lu-PSMA-617, compared against standard of care treatments for prostate cancer.[15,16] While highly effective, one limitation of these therapies is off-target toxicity, including xerostomia (dry mouth) and bone marrow suppression.[17] By combining the high selectivity of PSMA targeting with a spatially localized neutron beam, PSMA targeted BNCT has the potential to have high treatment efficacy with relative sparing of healthy tissues.

A prior report suggested that boron-labeled PSMA targeting agents could bind to prostate cancer cells with high affinity both *in vitro* and *in vivo*. However, improved delivery of boron would be required for effective BNCT.[10] A series of boron-labeled agents targeting PSMA had been designed and synthesized that demonstrated good to excellent binding affinity to PSMA *in vitro*. (previous study, data not available) The *in vivo* binding to PSMA was evaluated by a ^{68}Ga-PSMA-11 uptake blocking assay with PET imaging and biodistribution analysis.[18] The carborane-tagged small molecules could deliver only up to 4.2 μg boron/gram tumor in a prostate cancer xenograft mouse model, which needs significant improvement (>20 μg/g tissue) for effective BNCT.

Our hypothesis is based on prior reports suggesting that carborane-loaded poly(lactic-co-glycolic acid) (PLGA) nanoparticles can deliver significantly high boron content into the tumor tissue (>50 μg/g tissue), where the enhanced permeability and retention (EPR) effect would be highly prominent.[19] Besides, the block copolymer of PLGA and Polyethylene glycol (PEG) are known to be potent drug delivery systems in which the spontaneously formed polymeric nanoparticles with hydrophobic core accommodates sufficient quantity of hydrophobic drug molecules with controlled release, and the outer hydrophilic PEG corona protects the nanoparticles from immune surveillance.[20-24]

The nanoparticles were formulated using polymer conjugates and subsequently their size and the stabilities had been analyzed in different physiological conditions. *In vitro* studies such as blocking assay, competitive binding assay and cell boron uptakes were also performed. To assess the kinetics and biodistribution of the nanoparticle over time, ^{89}Zr, a positron emitting radionuclide, was attached to it. ^{89}Zr is an ideal radioisotope for labeling and studying nanoparticles as well as other biologically active molecules due to its relatively long half-life ($t_{1/2}$ = 78.4 hr.) and low energy positron emission. However, this report includes only the studies and data in which I was a part of the experiment.

Over the past few months, we have been assessing the *in vitro* boron release kinetics of o-carborane from nanoparticles and the *in vivo* biodistribution studies. Using ^{89}Zr labeled nanoparticles with and without PSMA targeting ligands, we have carried out micro-positron emission tomography – computed tomography (μPET-CT) imaging and biodistribution studies in PSMA (+) PC3-Pip and PSMA (-) PC3-Flu dual xenograft bearing mice models. We have performed the *in vivo* boron biodistribution studies and have also analyzed the PET imaging data by generating 3D free hand ROIs for few organs (heart, tumor, spleen, and liver) using the AMIDE software, which helped us

to perform quantitative analysis to assess the nanoparticle uptake at imaging time points. ROI statistical analysis were computed through the AMIDE software to assess the relevance of our findings.

The NPs with 75 w% PLGA-PEG-ACUPA conjugates showed significant binding affinity to PSMA (+) PC3-Pip cells to that of the NPs without any ACUPA ligands (control). However, the NPs suffer from a rapid release of carborane that could be assumed to suppress the targeted boron delivery both *in vitro* and *in vivo*. Although the PSMA (+) PC3-Pip tumor showed around 2-fold higher NPs uptake than in PSMA (-) PC3-Flu tumor, no improved uptake was witnessed for the ACUPA conjugated targeted NPs. Besides, the *in vivo* targeted boron delivery was found to be limited through this amphiphilic polymer NPs.

2. Methods

2.1. Materials and Instrumentation

PLGA-PEG-OMe (Catalog No. AK037) and PLGA-PEG-COOH (Catalog No. AI078) block copolymers were purchased from PolySciTech. ^{89}Zr oxalate was purchased from 3D Imaging and the Cyclotron Laboratory at the University of Wisconsin, Madison (Madison, WI). The radiolabeling chelator, p-Isothiocyanate-benzyl-DFO (catalog No. B-705), was purchased from Macrocyclics, Inc. o-Carborane was purchased from Boron Specialties (PA, U.S.A.). RPMI-1640 medium, fetal bovine serum (FBS), and penicillin−streptomycin solutions were purchased from Life Technologies (NY, U.S.A.). All other commercially available chemicals (building blocks, reagents, and solvents) were purchased as reagent grade from Sigma Aldrich, VWR, or Thermo Fisher Scientific and used as received.

2.2. Nanoparticle Synthesis

5 mg of PLGA-PEG conjugates and 10 w% of carborane were dissolved in 0.5 mL of DCM/Acetone (4:1 v/v). For preparing carborane solution, 100 mg of o-carborane was dissolved in 1 mL of DCM/acetone (4:1). 5μL (0.5 mg) was drawn from the solution. 0.5 mL of the polymer/carborane solution was added to 10 mL of DI water containing 0.1 % PVA. The solution was then sonicated for 1 min using a probe based 20 kHz sonicator at 80% amplitude. After sonication, the solution was stirred overnight in open to evaporate the organic solvents and stabilize the nanoparticles at room temperature. The dispersed nanoparticles were centrifuged twice at 16k rcf for 15 min and the solvent was replaced with DI water to remove any remaining organic solvents, excess PVA and non-capsulated carborane. Finally, all the pellets were redispersed in an appropriate amount of saline for required nanoparticle concentration ***(Fig. 3.1)***.

Three different nanoparticle formulations were synthesized and employed in this experiment, viz: DFB(25) NPs, DFB(25)ACUPA(25) NPs, and DFB(25)ACUPA(75) NPs.

2.3. In Vitro Drug Release Study of o-Carborane from Nanoparticles

Dialysis membrane was soaked in distilled water for 30 min at room temperature to remove the preservative after which it was rinsed thoroughly with distilled water. 5mg of nanoparticle in 0.5mL PBS was placed in a dialysis tubing cellulose membrane (molecular weight cut-off: 6-8 kDa) and was kept in the release medium of 100 mL of PBS (pH 7.4). The sample suspension was stirred at 30 rpm at 37ºC. At each time point like 0, 1h, 4h, 24h; 5µL of the nanoparticles from the dialysis membrane were added to 10mL of ICP matrix (2% H_2SO_4, 2% HNO_3, and 0.3% triton in Millipore water) and the released carborane concentration was calculated by analyzing the boron content with ICP-OES measurement. The readings were in triplicate.

2.4. Boron Analysis:

After the formulation of nanoparticles, the encapsulation of boron was determined by ICP-OES (Inductively Coupled Plasma – Optical Emission Spectrometry) analysis by diluting the sample in ICP matrix. The ICP matrix was prepared using 2% H_2SO_4, 2% HNO_3, and 0.3% triton in Millipore water.

2.5. In-Vitro Boron Uptake Studies

PC3-pip and PC3-flu cells were seeded in 6-well plates at around 1M cells/well for the next day experiment. Cells were washed twice with PBS, and 2.4 mL of fresh media was added with/without 1 mM PSMA-2 and incubated for 1 h at 37ºC. After 1 h, all the wells were added with 2.5 mg of the prepared nanoparticles in 100 mL of saline, which is supposed to have around 50 mg of carborane (considering 2 w% carborane encapsulation). After incubation for 1 h at 37ºC again, the

cells were washed with PBS two times. Then, the cells were treated with 200 μL of concentrated H_2SO_4 and HNO_3 each and kept at room temperature for 24 h. 30 mL of Triton-X-100 was added to the solution, and the whole solution was transferred to 15 mL conical tubes. Again, the wells were washed with 2 mL of DI water and subsequently transferred to the same conical tubes. Finally, the conical tubes were diluted to 10 mL with DI water. The boron content was measured by inductively coupled plasma optical emission spectrometry (ICP-OES, Thermo Scientific iCAP 7000).

2.6. Inoculation of mice with dual xenograft

All animal studies were conducted according to an Institutional Animal Care & Use Program (IACUC) approved protocol. Male mice that were 5−6 weeks old, housed under aseptic conditions, received subcutaneous dual tumor cell inoculation, as approved by the University of California, San Francisco Institutional Animal Care and Use Committee. The experiment was conducted on 12 immunocompromised mice. All the mice were implanted with dual xenograft PSMA (+) PC3-Pip and PSMA (-) PC3-Flu tumor cells, out of which 10 were advanced for μPET/CT imaging and biodistribution studies. All xenograft injections took place at the UCSF Preclinical Therapeutics Core. Approximately 3 million cells were implanted subcutaneously in 100μL of 1:1(v/v) serum free media and Matrigel (Fisher Scientific, IL) mixture were injected in the left (PC3-Pip) and the right (PC3-Flu) thigh of the animals. The xenografts were given ample time to grow and expand. The mice were injected with radiolabeled nanoparticle for μPET imaging and biodistribution analysis when the tumor reached a size of around 150-300mm^3.

2.7. In-vivo PET Imaging studies

For the μPET-CT imaging, the Siemens Inveon imaging system (Siemens, Germany) was utilized. The system comprises of two independent scanners: the Inveon dedicated PET (D-PET) and the Inveon multimodality scanner. μPET-CT provides both functional and anatomical information, allowing to assess the accumulation of the injected nanoparticle within the major organs and engrafted tumor on the mice models. Approximately 3 weeks after implantation, animals with tumors reaching optimum size (150-300mm^3) were anesthetized by isoflurane inhalation and the radiolabeled nanoparticles with and without PSMA ligand were administered via tail vein IV injection. The animals were then imaged by μPET/CT imaging system at 2 h, 20 h and 96 h time points post drug injection and image analysis was done. Image analysis, which so far remains my biggest contribution to the overall project, was completed using the multimodal medical image processing software, AMIDE (Loening, 2003). The PSMA (+) PC3-Pip and PSMA (-) PC3-Flu tumor bearing mice were sacrificed at the 96h time point post injection of the ^{89}Zr radiolabeled nanoparticle. Blood was collected by cardiac puncture. Major organs (brain, bone, heart, kidney, liver, lung, muscle, pancreas, spleen, and subcutaneous tumors) were harvested, weighed, and counted in an automated gamma counter (Hidex). The percent injected dose per gram of tissue (% ID/g) was calculated by comparison with standards of known radioactivity.

2.8. In Vivo Boron Biodistribution Studies

Approximately 3 weeks of inoculation, animals with tumors reaching 150-300 mm^3 were anesthetized by isoflurane inhalation and were administered with 20 mg respective nanoparticles in 200 μL of saline that contains ~400 mg carborane. The mice were sacrificed at 2 h, 20 h, and 96 h post-injection, and blood was collected by cardiac puncture. Major organs (brain, bone, heart,

kidney, liver, lung, muscle, pancreas, spleen, and subcutaneous tumor) were harvested and weighed. Tissue samples were digested for two days at room temperature in 1 mL of a 1:1 mixture of concentrated sulfuric and nitric acids. After digestion, 1.5 mL of a 5% Triton X-100 solution in water was added to each sample. The samples were then sonicated for 90 min. A 1 mL portion of the sample solution was transferred to a 15 mL centrifuge tube and diluted to 10 mL with ICP matrix. The samples were processed for boron analysis by ICP-OES.

2.9. Statistical Analysis

Data were analyzed using the unpaired, two-tailed Student's t-test and one-way ANOVA. Differences at the 95% confidence level ($P < 0.05$) were statistically significant.

3. Results

3.1. Formulation of carborane loaded nanoparticles:

The Poly(lactide-co-glycolide)-block-poly(ethylene glycol); PLGA-PEG block copolymer is known to self-assemble into nanoparticles wherein the hydrophobic biodegradable PLGA core allows the encapsulation and controlled release of hydrophobic carborane and the outer hydrophilic corona of PEG protects the nanoparticle from immune surveillance. In the simplest version of this carborane encapsulated nanoparticles, the free carboxyl groups at the PEG end conjugated with the PSMA inhibitor (PSMA-1) for targeted delivery of boron to the tumor site. After the synthesis of nanoparticles, the carborane encapsulation was quantified in the nanoparticles formulated with 10wt% of carborane by ICP-OES analysis. The nanoparticles were found to encapsulate 1.86 wt% of carborane.

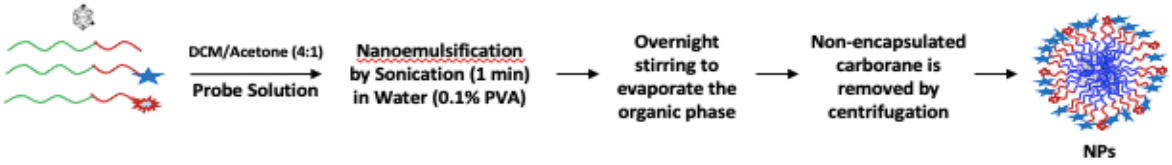

Figure 3.1: Brief step-by-step protocol for the synthesis of carborane loaded theranostic nanoparticles

As depicted in ***Fig 3.2***, three different NPs were formulated and radiolabeled with varying w% of polymer conjugates or PLGA-PEG-OMe and were subsequently subjected to *in vitro* and *in vivo* assessment.

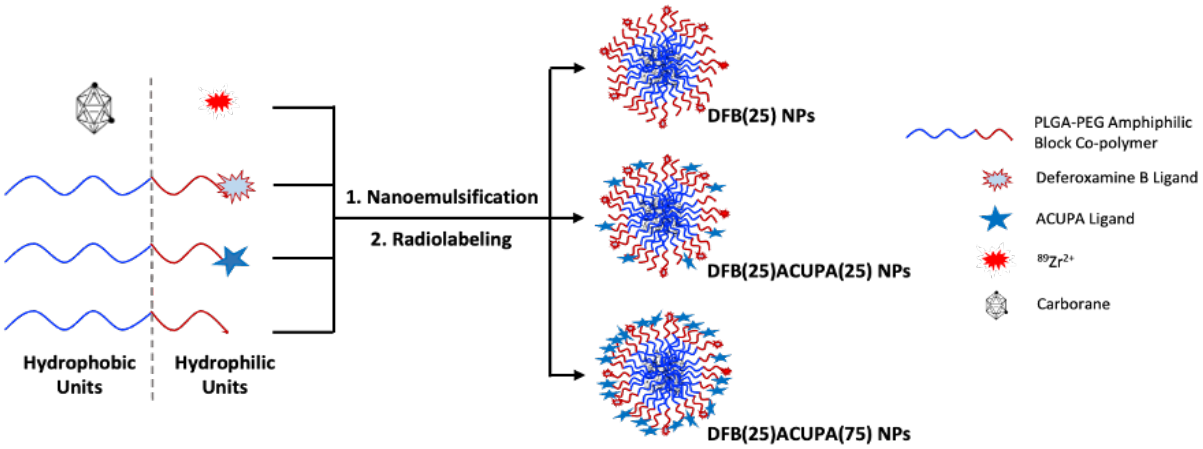

Fig 3.2. Representation of PLGA-PEG block copolymer-based amphiphilic nanoparticles for targeted delivery of boron.

PSMA-targeted NPs were formulated by dissolving 25 w% or 75 w% of PLGA-PEG-ACUPA copolymers, whereas all the NPs were included 25 w% of PLGA-PEG-DFB conjugates to efficiently chelate $^{89}Zr^{2+}$ for PET imaging. The detailed parameters for the nanoparticle formulation are presented in ***Fig.3.3.***

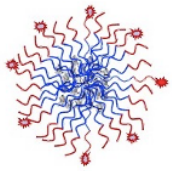

[^{89}Zr]DFB(25) NPs

Formulation Parameters for Control Nanoparticle

1.	PLGA	20 kDa
2.	PEG	5 kDa
3.	Carborane Content	10 Weight%
4.	PLGA-PEG-OMe	75 Mol%
5.	PLGA-PEG-DFB	25 Mol%
6.	Preparation Technique	Nano-emulsification
7.	Organic phase	DCM/Acetone
8.	PVA	0.1%

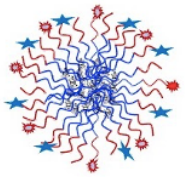

[^{89}Zr]DFB(25)ACUPA(25) NPs

Formulation Parameters for targeted Nanoparticle

1.	PLGA	20 kDa
2.	PEG	5 kDa
3.	Carborane Content	10 Weight%
4.	PLGA-PEG-OMe	50 Mol%
5.	PLGA-PEG-ACUPA	25 Mol%
6.	PLGA-PEG-DFB	25 Mol%
7.	Preparation Technique	Nano-emulsification
8.	Organic phase	DCM/Acetone
9.	PVA	0.1%

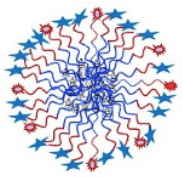

[^{89}Zr]DFB(25)ACUPA(75) NPs

Formulation Parameters for targeted Nanoparticle

1.	PLGA	20 kDa
2.	PEG	5 kDa
3.	Carborane Content	10 Weight%
4.	PLGA-PEG-OMe	50 Mol%
5.	PLGA-PEG-ACUPA	25 Mol%
6.	PLGA-PEG-DFB	25 Mol%
7.	Preparation Technique	Nano-emulsification
8.	Organic phase	DCM/Acetone
9.	PVA	0.1%

Fig 3.3. Detailed formulation parameters for the NPs.

3.2. Boron Encapsulation and In Vitro Drug Release

The boron encapsulation in the NPs was determined by ICP-OES measurement and was found to be around 1.86 w% by using ~7.5 w% of boron with respect to polymer weight. It was also observed that the boron encapsulation remained almost similar (1.92w%) even if the boron content added was increased to ~15 w%. The cumulative release of boron from NPs was evaluated by using a dialysis membrane of 6-8 kDa pore size in PBS at 37◦C (***Fig 3.4***).

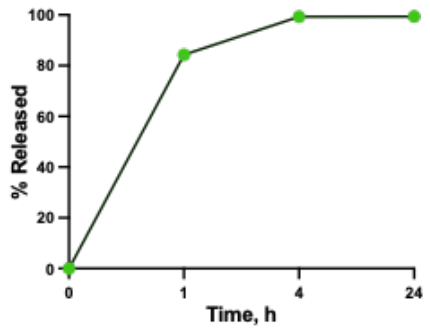

Fig 3.4 Boron release rate from PLGA-PEG NPs

It was observed that more than 84% of encapsulated boron was released from the NPs within 1 h, which increased up to 99% at 4 h. that demonstrated a fast release of carborane from the PLGA core.

3.3. In-Vitro Boron Uptake Studies

A cellular boron uptake assay was performed in both PC3-Pip and PC3-Flu using all the three NPs formulations, and the known PSMA-2 ligand was employed as a blocking agent (***Fig.3.5***). However, irrespective of the presence of PSMA targeting ACUPA ligands, both DFB(25)ACUPA(25) NPs and DFB(25)ACUPA(75) NPs were unable to demonstrate any improved boron uptake to that of the non-targeted DFB(25) NPs. This could be due to the fast

release of carborane from the NPs, and the boron uptake of around 0.6-0.8 %ID could be due to the non-specific uptake of the released carborane present in the media. The cellular uptake was 3.01 ± 0.18 %ID [^{89}Zr]DFB(25)ACUPA(75) NPs in PSMA expressing PC3-Pip cells, which was reduced to 1.97 ± 0.21 %ID by blocking a known high affinity PSMA binding agent (n = 3, mean ± SD, **P < 0.01, ***P < 0.001, Student's T-test). Overall, the DFB(25)ACUPA(75) nanoparticles demonstrated PSMA mediated cell binding *in vitro*, and therefore this formulation was advanced for *in vivo* imaging and biodistribution studies.

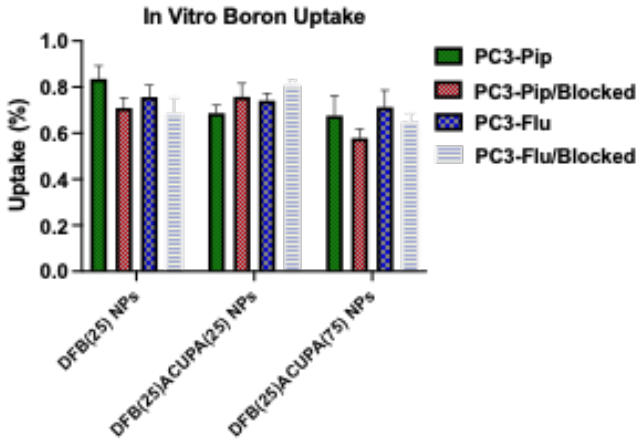

Fig 3.5. Boron uptake in both PC3-Pip and PC3-Flu cells using PSMA-2 ligand as blocking agent.

3.3. In vivo PET Imaging and Biodistribution:

The ability of the boron and ^{89}Zr labeled NPs to target PSMA *in vivo* was evaluated using PET imaging and biodistribution assay. The *in vivo* studies were performed in athymic mice bearing PC3-Pip and PC3-Flu dual xenografts ~3 weeks post-inoculation. For PET imaging, 200 µCi of the NPs ([^{89}Zr]DFB(25) NPs or ([^{89}Zr]DFB(25)ACUPA(75) NPs) were administered, and mice were imaged at multiple timepoints (2 h, 20 h, and 96 h) post intravenous injection. They were sacrificed for organ collection and gamma counting of tissues after 96 h timepoint imaging.

Fig. 3.6 shows trans axial micro-PET/CT images of mice injected with and without PSMA targeting ACUPA ligands of the NPs and ***Fig 3.7*** shows the maximum intensity projection images.

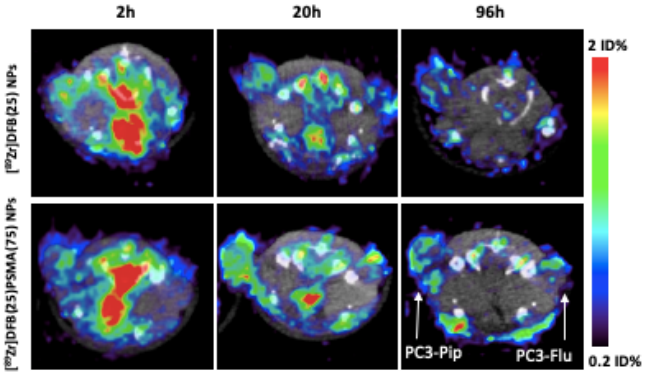

Fig 3.6: Axial fused micro-PET/CT imaging with ^{89}Zr radiolabeled NPs in male nu/nu mice with subcutaneous PC3-Pip and PC3-Flu xenografts.

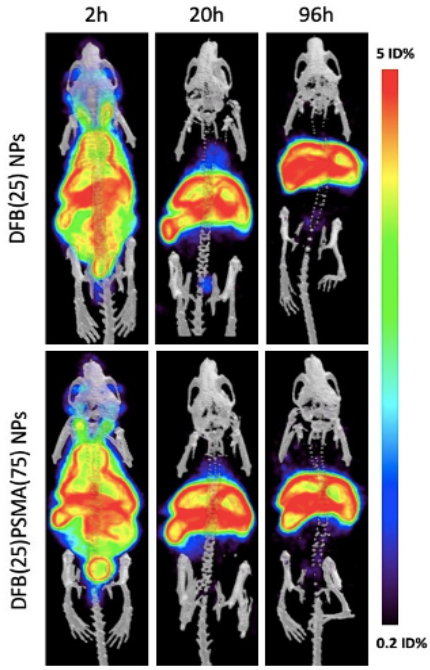

Fig.3.7. Maximum intensity projection of ^{89}Zr labeled NPs from 2 h to 96 h post injection.

All micro-PET/CT images were segmented into representative regions of interest ***(Table 3.1)*** and time activity curves were generated as shown in ***Fig 3.8-3.9***

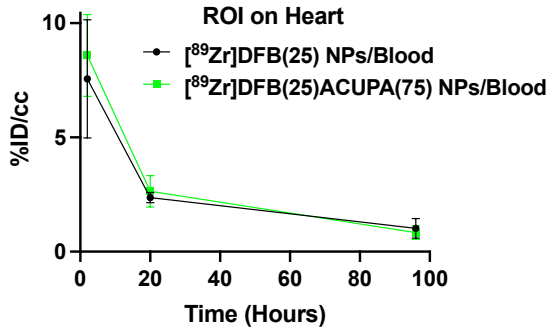

Fig 3.8. ROI plot for blood up to 96 h.

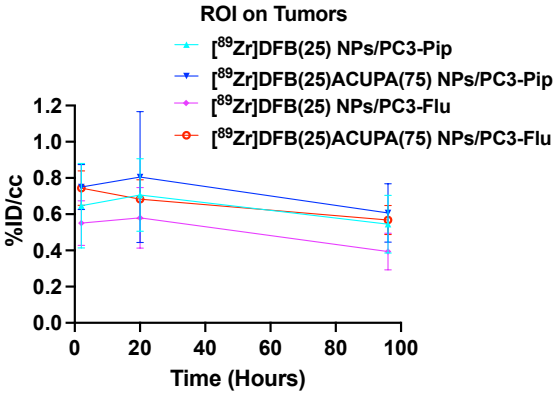

Fig 3.9. ROI plot for tumors up to 96 h.

Table 3.1. Region of interest analysis represented as mean ± standard deviation of tumor and heart for the micro PET/CT images at 2 h, 20 h, and 96 h.

	[89Zr]DFB(25) NPs			**[89Zr]DFB(25)ACUPA(75) NPs**		
Organs	**2h**	**20h**	**96h**	**2h**	**20h**	**96h**
Heart	8.588	3.482	1.016	7.556	3.88	0.826
Liver	13.178	13.876	13.55	12.84	11.78	12.58
Spleen	10.344	25.062	31.49	11.38	15.528	25.66
PC3 - Pip	0.744	0.802	0.6	0.642	0.7	0.54
PC3 - Flu	0.74	0.676	0.562	0.546	0.576	0.39

The ROI plots for the liver and spleen are shown below in ***Fig 3.10*** A higher uptake was seen in the organs like liver and spleen whereas a lower uptake was observed in the tumors.

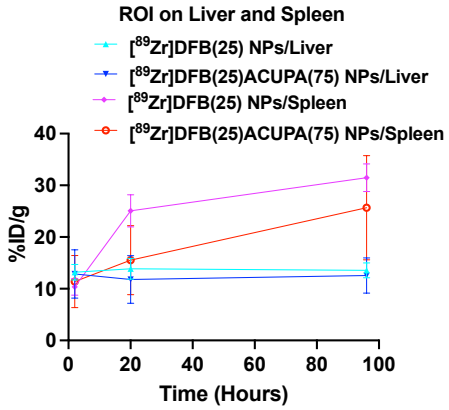

Fig. 3.10. ROI plot for liver and spleen up to 96 h.

While the tumor accumulation was observed to be below 1 %ID/gram for both the targeted and non-targeted NPs, a 2-fold higher tumor uptake was obtained in PSMA(+) PC3-Pip to that of the PSMA(-) PC3-Flu tumors that matched the ROI results and were in line with the biodistribution data obtained at 96 h ***Fig. 3.11-3.13***. Biodistribution analysis data in ID%/gram tissue for radiolabeled [^{89}Zr]DFB(25) NPs and [^{89}Zr]DFB(25)ACUPA(75) NPs at 96 h are shown in ***Table 3.2***

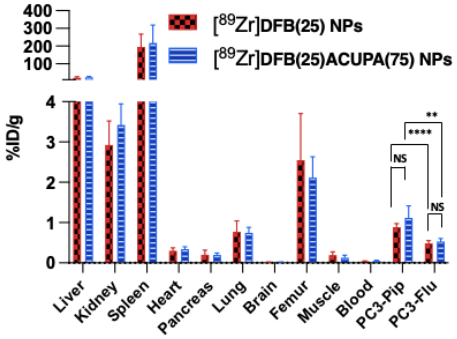

Fig.3.11. Biodistribution of ^{89}Zr radiolabeled NPs in various tissues at 96 h was determined by collecting organs and gamma counting (n = 5, mean ± SD, **P < 0.01, ****P < 0.0001, NS P > 0.05, Student's T-test)

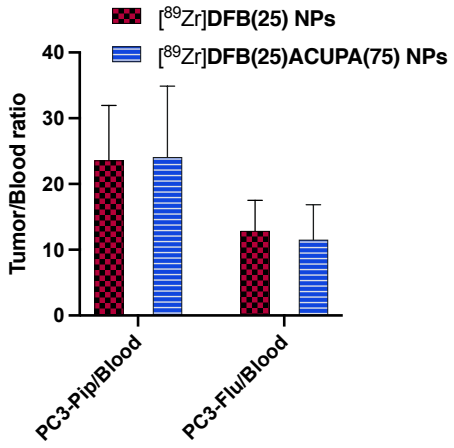

Fig.3.12. Tumor-to-blood and of ^{89}Zr radiolabeled NPs at 96 h. (n = 5, mean ± SD, **P < 0.01, ****P < 0.0001, NS P > 0.05, Student's T-test).

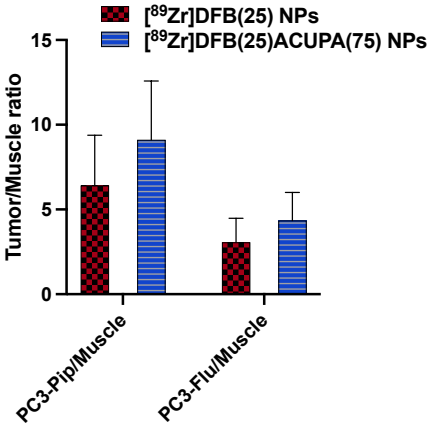

Fig.3.13. Tumor-to-muscle ratio of ^{89}Zr radiolabeled NPs at 96 h. (n = 5, mean ± SD, **P < 0.01, ****P < 0.0001, NS P > 0.05, Student's T-test).

However, there was no significant improvement in the uptake of targeted NPs as compared to the non-targeted. The 2-fold increase in the uptake in PSMA(+) PC3-Pip tumors to that of the PSMA(-) PC3-Flu tumors could be due to the difference in their enhanced permeability and retention (EPR) effect. [25,26]

Table 3.2 Biodistribution analysis data represented as mean ± standard deviation in ID%/gram tissue for radiolabeled [^{89}Zr]DFB(25) NPs and [^{89}Zr]DFB(25)ACUPA(75) NPs at 96 h.

Organs	[89Zr]DFB(25) NPs	[89Zr]DFB(25)ACUPA(75) NPs
Liver	20.8416	23.9474
Kidney	2.9278	3.1762
Spleen	194.31	205.8916
Heart	0.3022	0.3215
Pancreas	0.201	0.1973
Lung	0.7716	0.7571
Brain	0.017	0.0182
Femur	2.5502	2.3323
Muscle	0.1892	0.1596
Blood	0.0402	0.0458
PC3-Pip	0.8858	1.0015
PC3-Flu	0.4848	0.5067

3.4. In Vivo Boron Biodistribution

Finally, the *in vivo* boron delivery of the targeted and nontargeted nanoparticles was tested in the same dual PC3-Pip and PC3 flu xenograft model utilized for the PET imaging assay. The organs collected at 2 h, 20 h, and 96 h post-injection were subjected to ICP-OES to analyze boron uptake as shown in ***Fig. 3.14-3.16 and Table 3.3***.

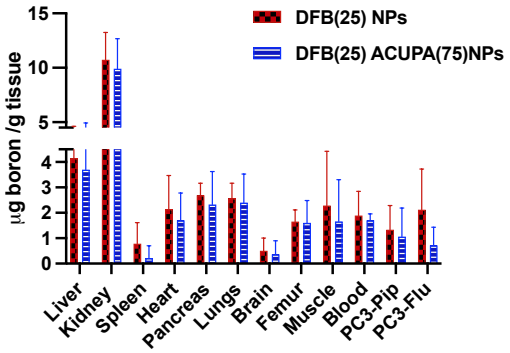

Fig 3.14. In vivo boron biodistribution at 2 h post-injection as determined by ICP-OES analysis. No boron could be detected in tissue at the 20h or 96h time points

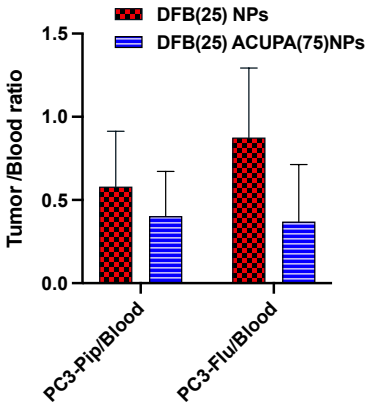

Fig.3.15 Tumor/blood uptake ratio of boron at 2 h post-injection.

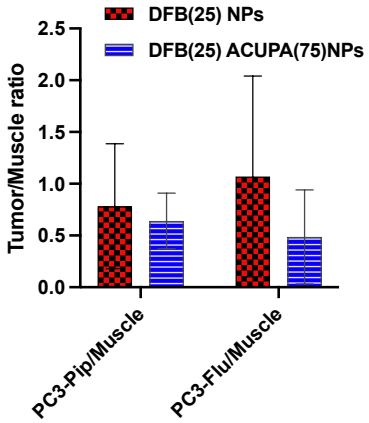

Fig. 3.16 Tumor/Muscle uptake ratio of boron at 2 h post-injection.

Table 3.3. In vivo boron biodistribution analysis data represented as mean ± standard deviation at 2 h post injection (μg/gram tissue).

Organs	[89Zr]DFB(25) NPs	[89Zr]DFB(25)ACUPA(75) NPs
Liver	4.148	3.692
Kidney	10.73	9.908
Spleen	1.297	1.08
Heart	2.138	1.694
Pancreas	2.688	2.3238
Lung	2.568	2.398
Brain	0.84	0.91
Femur	1.652	1.604
Muscle	2.855	2.075
Blood	1.892	1.702
PC3-Pip	1.66	1.3275
PC3-Flu	2.112	1.18667

Unexpectedly, the boron concentration in all the organ samples from 20 h and 96 h timepoint were below the detection limit. This suggested that a quick clearance of boron from the organs was observed. However, higher uptake was observed in the kidney than in the liver, suggesting primarily renal elimination. The tumor uptake remained within the window of approximately 1-2 μg/g of tissue, whereas the tumor/blood and tumor/muscle ratio were below 1. Overall, the biodistribution results demonstrated very little or no targeted boron delivery with PLGA-PEG NPs encapsulated with o-carborane.

4. Discussion

This report demonstrates the formulation of carborane encapsulated nanoparticles and quantification of the encapsulated boron was determined by ICP-OES analysis. By using the pre-synthesized PLGA-PEG-DFB and PLGA-PEG-PSMA conjugates, two different nanoparticles i.e. control (DFB(25)NPs) and targeted (DFB(25) PSMA(75)NPs) were formulated and tested for PET imaging. The boron content in the nanoparticles were different than other reports that demonstrated around 4.8-5.6 w% encapsulation of carborane in PLGA NPs.19 Overall, the results demonstrate that the PLGA-PEG-DFB conjugates were successfully synthesized and radiolabeled for *in vitro* and PET imaging analysis.

The targeted NPs (DFB(25) PSMA(75)NPs) demonstrated significantly higher binding affinity to PSMA in comparison to the control NPs. However, the PET imaging and the biodistribution results did not demonstrate any significant difference between the targeted and the non-targeted NPs. Although the overall tumor uptake was relatively low (~1 %ID), the tumor/blood ratio was around 25 for PC3-Pip tumor. A 2-fold higher uptake was seen in PSMA (+) PC3-Pip tumors than in the PSMA (-) PC3-Flu tumors, despite the presence or absence of the PSMA targeting ACUPA ligands. The difference in the uptake of both the tumors could be due to the EPR effect. It has been well demonstrated that the heterogeneous pore sizes in tumors mainly control the internalization of nanomedicine through the EPR effect, and the smaller size NPs with long circulating half-life is more receptive to maximize tumor uptake.27-30 In addition to this, a 2% ID/gram bone uptake was seen for both the NPs, which could be due to the weak nature of non-specific chelation of 89Zr2+ to the NPs.31

When the NPs were tested for boron delivery, it was observed that the nanoparticles released 84% of encapsulated boron within the first 1 h **(Fig.3.4)**. This fast release of carborane from the PLGA

core is in line with the prior report, where the PVA-coated PLGA NPs have been evaluated.19 The inferior loading and release kinetics of carborane could be due to its rigid molecular structure with the lesser surface area of interaction and provides weak non-covalent hydrophobic interaction with the PLGA unit. In line with these studies, the ACUPA conjugated NPs could not demonstrate targeted boron delivery to the PSMA(+) PC3-Pip cells either *in vitro* **(Fig. 3.5)** or *in vivo* **(Fig. 3.14 - 3.16)**.

The biodistribution of 89Zr tagged NPs showed significantly higher uptake in the liver and spleen, whereas the boron biodistribution studies showed higher boron uptake in the kidney to that of the liver and spleen. The observed distinct uptake of NPs and boron are in line with nature of materials used in this study A tumor boron uptake of at least 20−50 μg/g tumor tissue, accompanied by a tumor/muscle boron ratio of greater than 3:1 is required for effective tumor treatment by BNCT.1,3 However, the boron uptake did not reach the requirements, which implies that the current NPs formulations and/or dosing regimens are not sufficient for BNCT.

The results obtained suggested that the drug loading and release kinetics of the NPs were not suitable for successful BNCT. The *in vitro* cell binding assay and competition binding assay demonstrated relatively good PSMA binding affinity for the ACUPA conjugated NPs. However, their PSMA binding, and boron delivery *in vivo* were limited. One of the approaches to improve the boron loading and release kinetics and the *in vivo* stability of the NPs would be that the o-carborane could be covalently conjugated with hydrophobic alkyl chains to increase the magnitude of non-covalent hydrophobic interaction with PLGA, which could eventually enhance the encapsulation of o-carborane in the PLGA core and would allow a slower release.[32] The stability of the formulated NPs could be improved by using cross-link amphiphilic polymer which would

improve the release kinetics of o-carborane. These few improvements to the method represent important areas for future investigation.

5. Conclusion

In this study, a set of three theranostic NPs encapsulated with carborane were successfully formulated, characterized, and biologically evaluated for simultaneous PET imaging and targeted boron delivery to PCa for BNCT. Although the influence of the ACUPA ligands to bind PSMA *in vivo* was minimal, the NPs demonstrated 2-fold higher uptake in PSMA(+) PC3-Pip tumors with an impressive tumor/blood ratio. Due to the rapid release of carborane, the nanoparticles could not deliver high boron content to the PC3 tumors. In summary, the results obtained in this study would be helpful in future studies of PSMA targeted nanoparticles and in the development of boron delivery vehicles for a successful BNCT.

References

[1] Hu, K., et al. (2020). "Boron agents for neutron capture therapy." Coordination Chemistry Reviews **405**: 213139.

[2] Heber, E. M., et al. (2014). "Therapeutic efficacy of boron neutron capture therapy mediated by boron-rich liposomes for oral cancer in the hamster cheek pouch model." *Proc. Natl. Acad. Sci. U. S. A.*, **111**, 16077−16081. DOI https://doi.org/10.1073/pnas.1410865111.

[3] Barth, R.; Mi, P.; Yang, W., Boron delivery agents for neutron capture therapy of cancer. *Cancer Communications* **2018,** *38*.

[4] Haapaniemi, A.; Kankaanranta, L.; Saat, R.; Koivunoro, H.; Saarilahti, K.; Makitie, A.; Atula, T.; Joensuu, H., Boron Neutron Capture Therapy in the Treatment of Recurrent Laryngeal Cancer. *International Journal of Radiation Oncology Biology Physics* **2016,** *95* (1), 404-410.

[5] Nariai, T.; Ishiwata, K.; Kimura, Y.; Inaji, M.; Momose, T.; Yamamoto, T.; Matsumura, A.; Ishii, K.; Ohno, K., PET pharmacokinetic analysis to estimate boron concentration in tumor and brain as a guide to plan BNCT for malignant cerebral glioma. *Applied Radiation and Isotopes* **2009,** *67* (7-8), S348-S350.

[6] Schinazi, R.; Hurwitz, S.; Liberman, I.; Glazkova, Y.; Mourier, N.; Olson, J.; Keane, T., Tissue disposition of 5-o-carboranyluracil - A novel agent for the boron neutron capture therapy of prostate cancer. *Nucleosides Nucleotides & Nucleic Acids* **2004,** *23* (1-2), 291-306.

[7] Gifford, I.; Vreeland, W.; Grdanovska, S.; Burgett, E.; Kalinich, J.; Vergara, V.; Wang,

C.;Maimon, E.; Poster, D.; Al-Sheikhly, M., Liposome-based delivery of a boron-containing cholesteryl ester for high-LET particle-induced damage of prostate cancer cells: A boron neutron capture therapy study. *International Journal of Radiation Biology* **2014,** *90* (6), 480-485.

[8] Yasui, L.; Kroc, T.; Gladden, S.; Andorf, C.; Bux, S.; Hosmane, N., Boron neutron capture in prostate cancer cells. *Applied Radiation and Isotopes* **2012,** *70* (1), 6-12.

[9] Xuan, S.; Vicente, M.; HeyHawkins, E.; Teixidor, C., Recent Advances in Boron Delivery Agents for Boron Neutron Capture Therapy (BNCT). *Boron-Based Compounds: Potential and Emerging Applications in Medicine* **2018**, 298-342.

[10] Wang, S., et al. (2019). "Synthesis and Initial Biological Evaluation of Boron-Containing Prostate-Specific Membrane Antigen Ligands for Treatment of Prostate Cancer Using Boron Neutron Capture Therapy." *Molecular Pharmaceutics* **16**(9): 3831-3841.

[11] Johansson, J. E.; Andrén, O.; Andersson, S. O.; Dickman, P. W.; Holmberg, L.; Magnuson, A.; Adami, H. O. Natural history of early, localized prostate cancer. *J. Am. Med. Assoc.* **2004**, *291*, 2713−2719. https://www.cebm.net/wp-content/uploads/2015/09/Natural-History-of-Early-Localized-Prostate-Cancer.pdf.

[12] Perner, S.; Hofer, M. D.; Kim, R.; Shah, R. B.; Li, H.; Möller, P.; Hautmann, R. E.; Gschwend, J. E.; Kuefer, R.; Rubin, M. A. Prostate-specific membrane antigen expression as a predictor of prostate cancer progression. *Hum. Pathol*. **2007**, *38*, 696−701. DOI: https://doi.org/10.1016/j.humpath.2006.11.012.

[13] Maurer, T.; Eiber, M.; Schwaiger, M.; Gschwend, J. E. Current use of PSMA-PET in prostate cancer management. *Nat. Rev. Urol.* **2016**, *13*, 226−235. DOI: 10.1038/nrurol.2016.26.

[14] Hillier, S. M.; Maresca, K. P.; Femia, F. J.; Marquis, J. C.; Foss, C. A.; Nguyen, N.; Zimmerman, C. N.; Barrett, J. A.; Eckelman, W. C.; Pomper, M. G.; Joyal, J. L.; Babich, J. W. Preclinical evaluation of novel glutamate-urea-lysine analogues that target prostate-specific membrane antigen as molecular imaging pharmaceuticals for prostate cancer. *Cancer Res*. **2009**, *69*, 6932−6940. DOI: 10.1158/0008-5472.CAN-09-1682

[15] Kratochwil, C.; Bruchertseifer, F.; Giesel, F. L.; Weis, M.; Verburg, F. A.; Mottaghy, F.; Kopka, K.; Apostolidis, C.; Haberkorn, U.; Morgenstern, A. ^{225}Ac-PSMA-617 for PSMA-Targeted α-Radiation Therapy of Metastatic Castration-Resistant Prostate Cancer. *J. Nucl. Med*. **2016**, *57*, 1941-1944. DOI: 10.2967/jnumed.116.178673.

[16] Rahbar, K.; Ahmadzadehfar, H.; Kratochwil, C.; Haberkorn, U.; Schafers, M.; Essler, M.; Baum, R. P.; Kulkarni, H. R.; Schmidt, M.; Drzezga, A.; Bartenstein, P.; Pfestroff, A.; Luster, M.; Lutzen, U.; Marx, M.; Prasad, V.; Brenner, W.; Heinzel, A.; Mottaghy, F. M.; Ruf, J.; Meyer, P. T.; Heuschkel, M.; Eveslage, M.; Bogemann, M.; Fendler, W. P.; Krause, B. J. German multicenter study investigating 177Lu-PSMA-617 radioligand therapy in advanced prostate cancer patients. *J. Nucl. Med*. **2017**, *58*, 85−90. DOI: 10.2967/jnumed.116.183194.

[17] Kratochwil, C.; Giesel, F. L.; Stefanova, M.; Benešová, M.; Bronzel, M.; Afshar-Oromieh, A.; Mier, W.; Eder, M.; Kopka, K.; Haberkorn, U. PSMA-Targeted Radionuclide Therapy of Metastatic Castration-Resistant Prostate Cancer with ^{177}Lu-Labeled PSMA-617. *J. Nucl. Med*. **2016**, *57*, 1170-1176. DOI: 10.2967/jnumed.115.171397

[18] Wang, S.; Blaha, C.; Santos, R.; Huynh, T.; Hayes, T.; Beckford-Vera, D.; Blecha, J.; Hong, A.; Fogarty, M.; Hope, T.; Raleigh, D.; Wilson, D.; Evans, M.; VanBrocklin, H.; Ozawa, T.; Flavell, R., Synthesis and Initial Biological Evaluation of Boron-Containing Prostate-

Specific Membrane Antigen Ligands for Treatment of Prostate Cancer Using Boron Neutron Capture Therapy. *Molecular Pharmaceutics* **2019,** *16* (9), 3831-3841.

[19] Takeuchi, I.; Nomura, K.; Makino, K., Hydrophobic boron compound-loaded poly(L-lactide-co-glycolide) nanoparticles for boron neutron capture therapy. *Colloids and Surfaces B-Biointerfaces* **2017,** *159*, 360-365.

[20] Hrkach, J.; Von Hoff, D.; Ali, M.; Andrianova, E.; Auer, J.; Campbell, T.; De Witt, D.; Figa, M.; Figueiredo, M.; Horhota, A.; Low, S.; McDonnell, K.; Peeke, E.; Retnarajan, B.; Sabnis, A.; Schnipper, E.; Song, J.; Song, Y.; Summa, J.; Tompsett, D.; Troiano, G.; Hoven, T.; Wright, J.; LoRusso, P.; Kantoff, P.; Bander, N.; Sweeney, C.; Farokhzad, O.; Langer, R.; Zale, S., Preclinical Development and Clinical Translation of a PSMA-Targeted Docetaxel Nanoparticle with a Differentiated Pharmacological Profile. *Science Translational Medicine* **2012,** *4* (128).

[21] Chen, Z.; Tai, Z.; Gu, F.; Hu, C.; Zhu, Q.; Gao, S., Aptamer-mediated delivery of docetaxel to prostate cancer through polymeric nanoparticles for enhancement of antitumor efficacy. *European Journal of Pharmaceutics and Biopharmaceutics* **2016,** *107*, 130-141.

[22] Gu, F.; Zhang, L.; Teply, B.; Mann, N.; Wang, A.; Radovic-Moreno, A.; Langer, R.; Farokhzad, O., Precise engineering of targeted nanoparticles by using self-assembled biointegrated block copolymers. *Proceedings of the National Academy of Sciences of the United States of America* **2008,** *105* (7), 2586-2591.

[23] Afsharzadeh, M.; Hashemi, M.; Babaei, M.; Abnous, K.; Ramezani, M., PEG-PLA nanoparticles decorated with small-molecule PSMA ligand for targeted delivery of galbanic acid and docetaxel to prostate cancer cells. *Journal of Cellular Physiology* **2020,** *235* (5), 4618-4630.

[24] Valencia, P.; Hanewich-Hollatz, M.; Gao, W.; Karim, F.; Langer, R.; Karnik, R.; Farokhzad, O., Effects of ligands with different water solubilities on self-assembly and properties of targeted nanoparticles. *Biomaterials* **2011,** *32* (26), 6226-6233.

[25] Vera, D.; Fontaine, S.; VanBrocklin, H.; Hearn, B.; Reid, R.; Ashley, G.; Santi, D., PET Imaging of the EPR Effect in Tumor Xenografts Using Small 15 nm Diameter Polyethylene Glycols Labeled with Zirconium-89. *Molecular Cancer Therapeutics* **2020,** *19* (2), 673-679.

[26] MATSUMURA, Y.; MAEDA, H., A NEW CONCEPT FOR MACROMOLECULAR THERAPEUTICS IN CANCER-CHEMOTHERAPY - MECHANISM OF TUMORITROPIC ACCUMULATION OF PROTEINS AND THE ANTITUMOR AGENT SMANCS. *Cancer Research* **1986,** *46* (12), 6387-6392.

[27] Chauhan, V.; Jain, R., Strategies for advancing cancer nanomedicine. *Nature Materials* **2013,** *12* (11), 958-962.

[28] Chauhan, V.; Popovic, Z.; Chen, O.; Cui, J.; Fukumura, D.; Bawendi, M.; Jain, R., Fluorescent Nanorods and Nanospheres for Real-Time In Vivo Probing of Nanoparticle Shape-Dependent Tumor Penetration. *Angewandte Chemie-International Edition* **2011,** *50* (48), 11417-11420.

[29] Chauhan, V.; Stylianopoulos, T.; Martin, J.; Popovic, Z.; Chen, O.; Kamoun, W.; Bawendi, M.; Fukumura, D.; Jain, R., Normalization of tumor blood vessels improves the delivery of nanomedicines in a size-dependent manner. *Nature Nanotechnology* **2012,** *7* (6), 383-388.

[30] Stylianopoulos, T.; Jain, R., Design considerations for nanotherapeutics in oncology. *Nanomedicine-Nanotechnology Biology and Medicine* **2015,** *11* (8), 1893-1907.

[31] Abou, D.; Ku, T.; Smith-Jones, P., In vivo biodistribution and accumulation of Zr-89 in mice. *Nuclear Medicine and Biology* **2011,** *38* (5), 675-681.

[32] Liang, G.; Ren, F.; Gao, H.; Zhu, F.; Wu, Q.; Tang, B., Sticky nanopads made of crystallizable fluorescent polymers for rapid and sensitive detection of organic pollutants in water. *Journal of Materials Chemistry a* **2017,** *5* (5), 2115-2122.

Publishing Agreement

It is the policy of the University to encourage open access and broad distribution of all theses, dissertations, and manuscripts. The Graduate Division will facilitate the distribution of UCSF theses, dissertations, and manuscripts to the UCSF Library for open access and distribution. UCSF will make such theses, dissertations, and manuscripts accessible to the public and will take reasonable steps to preserve these works in perpetuity.

I hereby grant the non-exclusive, perpetual right to The Regents of the University of California to reproduce, publicly display, distribute, preserve, and publish copies of my thesis, dissertation, or manuscript in any form or media, now existing or later derived, including access online for teaching, research, and public service purposes.

DocuSigned by:
Suchi Dhirona
2069E6088D78421...
Author Signature

8/26/2021
Date